From Immersed Boundary Method to Immersed Continuum Method

X. Sheldon Wang

Department of Mathematical Sciences
New Jersey Institute of Technology
Newark, NJ 07102

CAMS Report 0506-7, Spring 2006

Center for Applied Mathematics and Statistics

NJIT

From Immersed Boundary Method to Immersed Continuum Method

X. Sheldon Wang

Associate Professor, Department of Mathematical Sciences, New Jersey Institute of Technology, Newark, NJ 07102, xwang@njit.edu

CAMS Report 0506-7

Abstract

The objective of this paper is to present an overview of the newly proposed immersed continuum method in conjunction with the traditional treatment of fluid-structure interaction problems, the immersed boundary method, the extended immersed boundary method, the immersed finite element method, and the fictitious domain method. In particular, the key aspects of the immersed continuum method in comparison with the immersed boundary method are discussed. The immersed continuum method retains the same strategies employed in the extended immersed boundary method and the immersed finite element method, namely, the independent solid mesh moves on top of a fixed or prescribed background fluid mesh, and employs fully implicit time integration with a matrix-free combination of Newton-Raphson and GMRES iterative solution procedures. Therefore, the immersed continuum method is capable of handling compressible fluid interacting with compressible solid. Several numerical examples are also presented to demonstrate that the proposed immersed continuum method is a good candidate for multi-scale and multi-physics modeling platform.

Key words: Extended Immersed Boundary Method, Immersed Finite Element Method, Reproducing Kernel Particle Method, Fluid-Structure Interaction, Navier-Stokes Equations, Protein Molecular Dynamics, Red Blood Cell, Aggregation, Coagulation, Microcirculation, Capillary, Immersed Boundary Method, and Immersed Continuum Method.

1 Introduction

For the past decades, significant efforts have been drawn to the development of computational tools for fluid-structure interaction (FSI) analysis. Early research on potential flow interacting with submerged structures includes

Zienkiewicz and Newton, 1969 [1], in the context of finite element methods (FEM); and Mei, 1978 [2] and Aranha, *et al.*, 1979 [3], using boundary element methods (BEM).

In linear acoustoelastic analysis, it has been widely reported that the displacement-based fluid elements employed in frequency or dynamic analysis exhibit spurious non-zero frequency circulation modes (Kiefling, 1976 [4]; Hamdi, *et al.*, 1978 [5]; and Olson and Bathe, 1983 [6]). Various approaches have been introduced to obtain improved formulations, including a 4-node element based on a reduced integration technique (Chen and Taylor, 1990 [7]), the displacement potential and pressure formulation (Morand and Ohayon, 1979 [8]), and the velocity potential formulation (Everstine, 1981 [9]; Olson and Bathe, 1985 [10]; and Felippa and Ohayon, 1990 [11]). The mixed displacement/pressure finite element formulation proposed by Wang and Bathe, 1997 [12] has been proven to be reliable and free of spurious non-zero frequencies.

Representative works in time integration stability analysis, impact computation, sloshing, space-time formulation, and arbitrary Lagrangian-Eulerian (ALE) formulation for FSI systems include Belytschko and Kennedy, 1976 [13]; Belytschko, 1980 [14]; Park, 1980 [15]; Belytschko and Mullen, 1981 [16]; Liu, 1981 [17]; Tezduyar, *et al.* 1992 [18]; Nomura and Hughes, 1992 [19]; Farhat, *et al.*, 1995 [20]; Bathe 1996 [21]; and Wang, 1999 [22]. Reviews on various finite element formulations for FSI systems are available in Morand and Ohayon, 1995 [23] and Bathe, 1996 [24] and 1998 [25]. Recently, based on the previous effort by Park and Felippa, 1980 [15], partitioned procedures have been introduced to the time-domain solution of aeroelastic problems (Piperno, *et al.*, 1995 [26]) and domain decomposition methods are implemented in order to fully exploit different single-domain solution algorithms and dynamical characteristics (Ghattas and Li, 1995 [27] and 1998 [28]). In practice, the staggered iteration between fluids and solids still remains the most popular procedure to obtain dynamic solutions.

The immersed boundary method was initially developed by Peskin, 1977 [29], in which, immersed elastic fibers with the same fluid density are modeled as a set of equivalent body forces in the Navier-Stokes equations. Since its inception, the immersed boundary method has been extended to a variety of problems, including design of prosthetic cardiac valves (McQueen and Peskin, 1985 [30]), swimming motions of marine worms (Fauci and Peskin, 1988 [31]), wood pulp fiber dynamics (Stockie and Wetton, 1999 [32]), wave propagation in cochlea (Beyer, 1992 [33]), and biofilm processes (Fogelson *et al.*, 1996 [34]). Recently, alternative procedures such the immersed interface method (LeVeque and Li, 1997 [35]) and the level set method (Sethian, 1996 [36]) have also been proposed to eliminate the numerical problems introduced by large motions of the immersed boundary. Furthermore, the effects of the flexibility, geometry, and mass of the immersed structures are amply demonstrated

through the works of many other researchers [37] [38] [39] [40].

Immersed methods overcome many numerical problems such as severe fluid mesh distortions encountered in traditional finite element methods (FEM) and computational fluid dynamics (CFD) procedures when modeling very flexible immersed structures [22] [41] [42] [43] [44]. With immersed methods, the issue of fluid mesh updates is resolved. However, in current immersed methods, complex structures/solids are still represented by elastic fiber networks. In the proposed immersed continuum method, sophisticated nonlinear finite element formulations will be used.

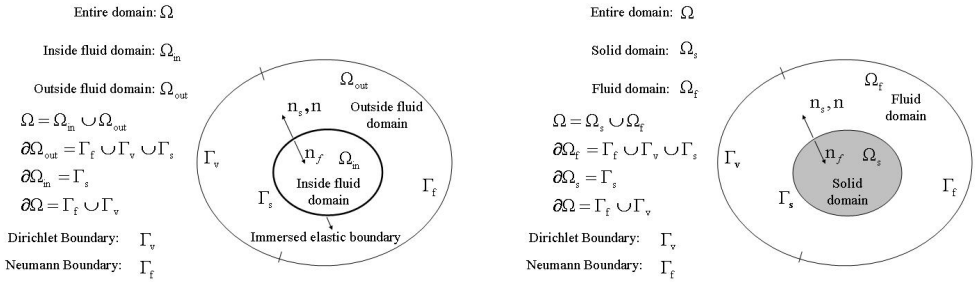

(a) Immersed Boundary (b) Immersed Continuum

Fig. 1. Illustrations of Immersed Boundary and Immersed Continuum.

In Section 2, we prove the equivalence of the immersed boundary (IB) method (Peskin, 1977 [29]) to the traditional treatment of fluid-structure interactions by matching the kinematic and dynamic boundary conditions around the fluid-structure interface. In Section 3, we also show the theoretical foundations for the extended immersed boundary method (Wang and Liu, 2004 [45]) and immersed finite element method (Zhang *et al.*, 2004 [46]). In addition, after a brief review of the fictitious domain approach (Glowinski *et al.*, 2001 [47]), we compare the immersed boundary method and its extensions with the fictitious domain approach. In Section 4, the newly proposed immersed continuum method (ICM) is presented to take into consideration of the compressibility of the submerged solid. This formulation retains the same strategies as in the extended immersed boundary method (EIBM) and immersed finite element method (IFEM), namely, the independent solid mesh moves on top of a fixed background fluid mesh. Several numerical examples are also presented for illustrative purposes in Section 5.

2 Immersed Boundary Method Recast in FEM

The immersed boundary method is recast in the principle of virtual work, which to the author's best knowledge, is the first attempt. This recast not only demonstrates why the immersed boundary method works but also points to the linkage between the fictitious domain method and the proposed immersed continuum methods.

In Fig. 1, typical immersed boundary and immersed continuum systems are used to illustrate the difference between the current immersed methods which primarily handle immersed fibers and fiber networks and the proposed new methods which deal with arbitrary immersed structures/solids with finite volume and mass. The strong and weak forms which are the foundations for finite element procedures will be discussed based on the illustrations in Fig. 1.

Consider a fluid domain Ω enclosed with a sufficiently smooth boundary, $\partial\Omega = \Gamma_v \cup \Gamma_f$, where Γ_v and Γ_f stand for the Dirichlet and Neumann boundaries, respectively. Suppose there exists an enclosed elastic boundary Γ_s (a line for two-dimensional cases and a surface for three-dimensional cases), the fluid domain Ω is separated into two regions, namely, the interior region Ω_i and the exterior region Ω_e. Therefore, the boundaries of the interior and the exterior regions can be simply expressed as $\partial\Omega_i = \Gamma_s$ and $\partial\Omega_e = \Gamma_s \cup \Gamma_v \cup \Gamma_f$. Denote $\boldsymbol{\sigma}$ as the stress tensor, $\mathbf{v}$ as the velocity vector, and ρ as the density in the fluid domain, the following governing equations (strong form) can be established:

$$\rho\dot{v}_i = \sigma_{ij,j} + f_i^{ext}, \text{ in } \Omega_i(\text{or } \Omega \setminus \Omega_e), \tag{2.1}$$
$$\rho\dot{v}_i = \sigma_{ij,j} + f_i^{ext}, \text{ in } \Omega_e, \tag{2.2}$$
$$[v_i] = 0, \text{ on } \Gamma_s, \text{ kinematic matching}, \tag{2.3}$$
$$[\sigma_{ij}n_j] = f_i^s + m\ddot{u}_i^s, \text{ on } \Gamma_s, \text{ dynamic matching}, \tag{2.4}$$

where the external body force $\mathbf{f}^{ext}$ will be replaced by $\rho\mathbf{g}$, with $\mathbf{g}$ as the gravitational acceleration; $\mathbf{f}^s$ and m stand for the elastic force and the mass density of the immersed boundary Γ_s (per unit length for two-dimensional cases and per unit area for three-dimensional cases); $\mathbf{u}^s$ denotes the interface displacement; and the surface normal vector $\mathbf{n}$ is aligned with that of the interior fluid domain $\mathbf{n}^i$ and opposite to that of the exterior fluid domain $\mathbf{n}^e$.

At this point, we can derive a number of numerical approaches to solving Eqs. (2.1) to (2.4). A straightforward approach is to represent the exterior and the interior fluid domains with different meshes and to match them accordingly at the interface Γ_s. This approach represents the traditional treatment of fluid-structure interaction problems, in which the solid mesh is coupled with the fluid mesh around the fluid-structure interface [42] [44].

Define the Sobolev space $[H^1_{0,\Gamma_v}(\Omega)]^d = \{\mathbf{w}| \quad \mathbf{w} \in [H^1(\Omega)]^d, \mathbf{w}|_{\Gamma_v} = \mathbf{0}\}$, where d represents the spatial dimensions, we express Eqs. (2.1) to (2.4) in the variational forms (weak form): $\forall \mathbf{w} \in [H^1_{0,\Gamma_v}(\Omega)]^d$

$$\int_{\Omega_i} w_i[\rho(\dot{v}_i - g_i) - \sigma_{ij,j}]d\Omega + \int_{\Omega_e} w_i[\rho(\dot{v}_i - g_i) - \sigma_{ij,j}]d\Omega = 0. \tag{2.5}$$

Remark 2.1 *In the variational forms,* $\mathbf{w} \in [H^1_{0,\Gamma_v}(\Omega)]^d$ *implies that the kinematic matching at the interface* Γ_s*, written as Eq. (2.3) is satisfied for all* $\mathbf{w}$*.*

Furthermore, using integration by parts and the divergence theorem, introducing the dynamic matching at the interface Γ_s, and combining the interior and exterior fluid domains with $\Omega_e \cup \Omega_i = \Omega$, Eq. (2.5) can be rewritten as: $\forall \mathbf{w} \in [H^1_{0,\Gamma_v}(\Omega)]^d$

$$\int_{\Omega}[w_i\rho(\dot{v}_i - g_i) + w_{i,j}\sigma_{ij}]d\Omega + \int_{\Gamma_s} w_i^s(f_i^s + m\ddot{u}_i^s)d\Gamma - \int_{\Gamma_f} w_i f_i^{\Gamma_f} d\Gamma = 0. \tag{2.6}$$

Remark 2.2 *In Eq. (2.6), the term involving the given surface traction* $\mathbf{f}^{\Gamma_f}$ *will remain the same as if the variational forms are carried out for the entire fluid domain instead of the interior and exterior parts. Thus the focus will be on the submerged interface* Γ_s*.*

Remark 2.3 *In Eq. (2.6), the external work comes from the external body force* $\mathbf{f}^{ext}$*, the surface traction* $\mathbf{f}^{\Gamma_f}$ *at the Neumann boundary* Γ_f*, and the elastic and inertial forces around the submerged interface* Γ_s*. Moreover, in Eq. (2.6), we do not stipulate the material derivative* $\dfrac{d\mathbf{v}}{dt}$ *and the stress* $\boldsymbol{\sigma}$*. Hence the turbulent and the non-Newtonian fluid models can eventually be incorporated. Finally, the kinematic matching at the submerged interface* Γ_s *also implies that the submerged interface will move at the same velocity as that of the fluid particles in the immediate vicinity. This important point marks the underlining connection between the traditional computational mechanics approaches, the immersed boundary method, and the fictitious domain method.*

In the immersed boundary method, we introduce the following two key equations:

$$f_i^{FSI} = -\int_{\Gamma_s} (f_i^s + m\ddot{u}_s)\delta(\mathbf{x} - \mathbf{x}^s)d\Gamma, \tag{2.7}$$

$$v_i^s = \int_{\Omega} v_i\delta(\mathbf{x} - \mathbf{x}^s)d\Omega, \tag{2.8}$$

where $\mathbf{f}^{FSI}$ is the so-called equivalent body force.

Remark 2.4 *In both Eqs. (2.7) and (2.8), the Dirac delta function is positioned at the current interface position* $\mathbf{x}^s$*. Before the discretization of the Dirac delta function, Eq. (2.8) can be simply interpreted as the evaluation of the fluid velocity at the submerged interface. In the discretized form, the Dirac delta function in Eq. (2.8) is equivalent to the shape function or kernel of the meshfree method.*

Note that Γ_s represents the current configuration of the submerged interface, and nonlinear mechanics is employed to relate the elastic force $\mathbf{f}^s$ with the interfacial position $\mathbf{x}^s$ or the displacement $\mathbf{u}^s$. It is also clear that as long as we use the same delta function for both Eqs. (2.7) and (2.8), the virtual power input from the submerged elastic boundary (or the immersed boundary) to the fluid domain can be expressed as

$$\int_\Omega w_i f_i^{FSI} d\Omega = -\int_{\Gamma_s}\int_\Omega w_i \delta(\mathbf{x}-\mathbf{x}^s)(f_i^s + m\ddot{u}_i^s) d\Omega d\Gamma = -\int_{\Gamma_s} w_i^s (f_i^s + m\ddot{u}_i^s) d\Gamma. \tag{2.9}$$

Because Eq. (2.9) holds for all $\mathbf{w} \in [H^1_{0,\Gamma_v}(\Omega)]^d$, the effect of the submerged elastic boundary can be simply replaced with the equivalent body force $\mathbf{f}^{FSI}$. Hence the governing equations (2.1) to (2.4) can be rewritten as

$$\rho\dot{v}_i = \sigma_{ij,j} + \rho g_i + f_i^{FSI}, \text{ in } \Omega; \tag{2.10}$$

and the variational equations (2.5) and (2.6) are modified as

$$\int_\Omega [w_i(\rho\dot{v}_i - \rho g_i - f_i^{FSI}) + w_{i,j}\sigma_{ij}] d\Omega - \int_{\Gamma_f} w_i f_i^{\Gamma_f} d\Gamma = 0. \tag{2.11}$$

Remark 2.5 *Eq. (2.11) provides us with the foundation of the key advantage of the alternative solution strategies for immersed boundaries or continua, namely, the independent solid mesh moves on top of a fixed background fluid mesh. Moreover, we must also point out that the so-called fixed background fluid mesh could also include the arbitrary Lagrangian-Eulerian (ALE) mesh with a prescribed mesh motion. In practice, such a mesh motion could follow the moving structures or solids as well as conform to the boundary deformation.*

Similarly, we can extend such a study to the extended immersed boundary method and the immersed finite element method. Consider the same domain Ω, suppose there exists a submerged solid domain Ω_s enclosed by a sufficiently smooth boundary Γ_s (a line for two-dimensional cases and a surface for three-dimensional cases), the entire domain Ω is subdivided into two regions, namely, the solid region Ω_s and the fluid region Ω_f. Therefore, the boundaries of the solid and the fluid regions can be simply expressed as $\partial\Omega_s = \Gamma_s$ and $\partial\Omega_f = \Gamma_s \cup \Gamma_v \cup \Gamma_f$. Denote $\boldsymbol{\sigma}$ as the stress tensor, $\mathbf{v}$ as the velocity vector, we establish the following governing equations (strong form):

$$\rho_s \dot{v}_i^s = \sigma_{ij,j}^s + \rho_s g_i, \text{ in } \Omega_s, \tag{3.12}$$

$$\rho_f \dot{v}_i^f = \sigma_{ij,j}^f + \rho_f g_i, \text{ in } \Omega_f, \tag{3.13}$$

$$[v_i] = 0, \text{ on } \Gamma_s, \text{ kinematic matching}, \tag{3.14}$$

$$[\sigma_{ij} n_j] = 0, \text{ on } \Gamma_s, \text{ dynamic matching}, \tag{3.15}$$

where the surface normal vector $\mathbf{n}$ is aligned with that of the solid domain $\mathbf{n}^s$ and opposite to that of the fluid domain $\mathbf{n}^f$.

Note that we use the subscript (for scalars) or the superscript (for vectors) s and f represent the solid and fluid domains, respectively. Define the same Sobolev space $[H^1_{0,\Gamma_v}(\Omega)]^d$, we express Eqs. (3.12) to (3.15) in the variational forms (weak forms): $\forall \mathbf{w} \in [H^1_{0,\Gamma_v}(\Omega)]^d$

$$\int_{\Omega_s} w_i[\rho_s(\dot{v}_i^s - g_i) - \sigma_{ij,j}^s]d\Omega + \int_{\Omega_f} w_i[\rho_f(\dot{v}_i^f - g_i) - \sigma_{ij,j}^f]d\Omega = 0. \tag{3.16}$$

Remark 3.1 $\mathbf{w} \in [H^1_{0,\Gamma_v}(\Omega)]^d$ *also implies that the kinematic matching of Eq. (3.14) is satisfied for all* $\mathbf{w}$.

Again, using integration by parts and the divergence theorem, introducing the dynamic matching at the interface Γ_s, and combining the solid and fluid domains with $\Omega_s \cup \Omega_f = \Omega$, Eq. (3.16) can be rewritten as: $\forall \mathbf{w} \in [H^1_{0,\Gamma_v}(\Omega)]^d$

$$\int_{\Omega} [w_i \rho_f(\dot{v}_i - g_i) + w_{i,j}\sigma_{ij}]d\Omega - \int_{\Gamma_f} w_i f_i^{\Gamma_f} d\Gamma - \int_{\Omega_s} w_i^s f_i^s d\Omega = 0, \tag{3.17}$$

with

$$\int_{\Omega_s} w_i^s f_i^s d\Omega = -\int_{\Omega_s} [w_i(\rho_s - \rho_f)(\dot{v}_i - g_i) + w_{i,j}(\sigma_{ij}^s - \sigma_{ij}^f)] d\Omega. \tag{3.18}$$

Remark 3.2 *In Eq. (3.15), the unit surface normal vectors at the fluid-solid interface Γ_s are assigned as $\mathbf{n}^s = -\mathbf{n}^f = \mathbf{n}$; whereas in Eq. (3.18) the term involving the given surface traction $\mathbf{f}^{\Gamma_f}$ will remain the same if the variational forms are carried out for the entire domain Ω instead of the solid and fluid parts. Thus the focus will be on the submerged solid Ω_s and its interface with the fluid Γ_s.*

Remark 3.3 *In Eq. (3.17), within the entire domain Ω, the external work comes from the external body force $\rho_f \mathbf{g}$, and the surface traction $\mathbf{f}^{\Gamma_f}$ at the Neumann boundary Γ_f; whereas the power input within the submerged solid domain Ω_s includes the contribution from the inertial force difference, the buoyancy force, and the internal energy difference. Again, the kinematic matching at the submerged interface Γ_s also implies that the submerged interface will move at the same velocity as that of the fluid particles in the immediate vicinity. In Eq. (3.17), we again do not stipulate the material derivative $\dfrac{d\mathbf{v}}{dt}$ and the stress $\boldsymbol{\sigma}$. Hence the turbulent and the non-Newtonian fluid models can eventually be incorporated.*

Just as in the immersed boundary method, in the extended immersed boundary method [45] and the immersed finite element method [46], we introduce the following two key equations to synchronize the fluid occupying the submerged solid domain Ω_s with the solid and distribute the solid force $\mathbf{f}^s$:

$$f_i^{FSI} = \int_{\Omega_s} f_i^s \delta(\mathbf{x} - \mathbf{x}^s) d\Omega, \tag{3.19}$$

$$v_i^s = \int_{\Omega} v_i \delta(\mathbf{x} - \mathbf{x}^s) d\Omega, \tag{3.20}$$

where $\mathbf{f}^{FSI}$ represents the same equivalent body force as in the immersed boundary method.

Note that $\mathbf{f}^s$ is the force density within the solid domain Ω_s; whereas $\mathbf{f}^{FSI}$ is the equivalent body force over the entire domain Ω. The physical significance of $\mathbf{f}^s$ and $\mathbf{f}^{FSI}$ is quite different. As a consequence, the entire fluid-solid interaction system is represented with the same governing equations (2.10) (strong form) and the corresponding variational form (2.11) (weak form).

Remark 3.4 *In Eq. (3.18), $\mathbf{f}^s$ can be considered as the equivalent force density within the submerged solid domain Ω_s. In fact, this force density directly corresponds to the rigid link between the fluid occupying the submerged solid domain Ω_s and the solid. In other words, the force density $\mathbf{f}^s$ stands for the*

Lagrangian multiplier corresponding to the constraint in Eq. (3.20). Of course, the definition in Eq. (3.18) also matches the virtual power input from the submerged solid domain Ω_s.

Note that the inertial force difference $-\int_{\Omega_s} w_i(\rho_s - \rho_f)\dot{v}_i d\Omega$ of the submerged solid continuum corresponds to the inertial force $-\int_{\Gamma_s} w_i^s m\ddot{u}_i^s d\Gamma$ of the submerged elastic boundary; whereas the internal energy difference $-\int_{\Omega_s} w_{i,j}(\sigma_{ij}^s - \sigma_{ij}^f)d\Omega$ of the submerged solid continuum corresponds to the elastic force $-\int_{\Gamma_s} w_i^s f_i^s d\Gamma$ of the submerged elastic boundary. In comparison with the submerged elastic boundary, the contribution of the submerged solid includes an additional term to account for the external body force difference (the so-called buoyancy) $\int_{\Omega_s} w_i(\rho_s - \rho_f)g_i d\Omega$. This buoyancy force is the direct manifestation of the submerged solid which unlike the submerged elastic boundary occupies a finite volume. Likewise, the inertial effect of the submerged solid includes the difference between the solid and fluid densities assuming the fluid occupying the submerged solid domain is forced to have the same motions as those of the solid.

It is important to point out that the essence of the extended immersed boundary method and the immersed finite element method is to introduce the same fluid in the submerged solid domain. Because such a volume of fluid does not exist physically, to account for the correct effect of the submerged solid exerting on the surrounding fluid, we must subtract the inertial force, the external body force, and the internal stress effects of such an imaginary fluid volume Ω_s. Moreover, for a fluid volume moving with an elastic body, the induced fluid stress in general is significantly smaller than the corresponding solid stress.

Eqs. (3.19) and (3.20) in EIBM/IFEM are comparable to Eqs. (2.7) and (2.8) in the IB method. Before we present the newly developed immersed continuum method for compressible solid interacting with compressible fluid, we would like first to summarize the main ideas in the fictitious domain method [47], another alternative formulation for immersed boundaries and continua.

Suppose there exists a rigid cylinder (for two-dimensional cases) or a rigid sphere (for three-dimensional cases) occupying a volume Ω_s in the total domain Ω. Again, around the fluid-solid interface Γ_s, the unit normal vector of the solid is $\mathbf{n}^s = \mathbf{n}$ which points outward to the flow region and the unit normal vector of the fluid is $\mathbf{n}^f = -\mathbf{n}$ which points inward to the submerged solid. Following the no-slip boundary condition on the interface Γ_s, we have

$$\mathbf{v}(\mathbf{x}, t) = \bar{\mathbf{v}}(t) + \bar{\boldsymbol{\omega}}(t) \times (\mathbf{x} - \bar{\mathbf{x}}(t)), \forall \mathbf{x} \in \Gamma_s, \tag{3.21}$$

where $\bar{\mathbf{x}}$, $\bar{\mathbf{v}}$, $\bar{\boldsymbol{\omega}}$, and $\mathbf{x}$ stand for the current position of the mass center, the velocity, and the angular velocity, and the position on the interface of the rigid body.

Because the solid occupying Ω_s is a rigid body, Eq. (3.21) can be rewritten as

$$\mathbf{v}(\mathbf{x}^s, t) = \bar{\mathbf{v}}(t) + \bar{\boldsymbol{\omega}}(t) \times (\mathbf{x}^s - \bar{\mathbf{x}}(t)), \forall \mathbf{x}^s \in \Omega_s. \tag{3.22}$$

Of course, on the fluid-solid interface Γ_s, Eq. (3.22) is manifested as Eq. (3.21). Furthermore, the governing equations (strong form) of the fluid-solid system can be depicted as

$$\rho_f \dot{v}_i = \sigma_{ij,j} + \rho_f g_i, \text{ in } \Omega_f, \tag{3.23}$$

$$M\dot{\bar{v}}_i = Mg_i + F_i^s, \text{ for the rigid body } \Omega_s, \tag{3.24}$$

$$\mathbf{I}\dot{\bar{\boldsymbol{\omega}}} + \bar{\boldsymbol{\omega}} \times \mathbf{I}\bar{\boldsymbol{\omega}} = \mathbf{T}^s, \tag{3.25}$$

where $\mathbf{I}$ and M are the rotational inertia tensor (or matrix) and the mass of the rigid body, respectively; and the resultant torque $\mathbf{T}^s$ and force $\mathbf{F}^s$ due to the fluid traction around the rigid body are expressed as

$$\mathbf{T}^s = -\int_{\Gamma_s} (\mathbf{x}^s - \bar{\mathbf{x}}) \times \boldsymbol{\sigma}\mathbf{n} d\Gamma, \tag{3.26}$$

$$\mathbf{F}^s = -\int_{\Gamma_s} \boldsymbol{\sigma}\mathbf{n} d\Gamma. \tag{3.27}$$

Similar to the approach in EIBM/IFEM, in the fictitious domain method, an imaginary fluid is introduced to occupy the submerged solid domain Ω_s and to synchronize with the solid within Ω_s. With the fluid velocity variation $\mathbf{w} \in [H^1_{0,\Gamma_v}(\Omega)]^d$, the rigid body velocity variation $\bar{\mathbf{w}} \in R^d$, and the rigid body angular velocity variation $\bar{\boldsymbol{\theta}} \in R^d$, combining the solid domain with the fluid domain, employing integration by parts, the divergence theorem, and Eqs. (3.22), (3.26), and (3.27), we can convert the governing equations (strong form) in Eqs. (3.23) to (3.25) into the variational equations (weak form),

$$\int_\Omega [\rho_f w_i(\dot{v}_i - g_i) + w_{i,j}\sigma_{ij}] d\Omega + r[M(\dot{\bar{v}}_i - g_i)\bar{w}_i + (\mathbf{I}\dot{\bar{\boldsymbol{\omega}}} + \bar{\boldsymbol{\omega}} \times \mathbf{I}\bar{\boldsymbol{\omega}}) \cdot \bar{\boldsymbol{\theta}}] = 0, \tag{3.28}$$

with $r = 1 - \rho_f/\rho_s$.

The key treatment in the immersed boundary method, the extended immersed boundary method, and the immersed finite element method, is to introduce

the delta function to synchronize the fluid motion with the solid motion within the immersed solid domain Ω_s, namely,

$$\mathbf{v}^s = \mathbf{v}^f. \tag{3.29}$$

In fact, the constraint of Eq. (3.29) introduces the (distributed) Lagrangian multiplier as the equivalent body force. In the fictitious domain method, a similar (distributed) Lagrangian multiplier $\boldsymbol{\lambda}$ is introduced, along with the following traditional mixed formulation, we obtain, $\forall \mathbf{w} \in [H^1_{0,\Gamma_v}(\Omega)]^d$ and $\boldsymbol{\lambda} \in [H^1(\Omega_s)]^d$

$$\begin{aligned} &\int_\Omega [\rho_f w_i(\dot{v}_i - g_i) + w_{i,j}\sigma_{ij}]d\Omega + r[M(\dot{\bar{v}}_i - g_i)\bar{w}_i + (\mathbf{I}\dot{\bar{\boldsymbol{\omega}}} + \bar{\boldsymbol{\omega}} \times \mathbf{I}\bar{\boldsymbol{\omega}}) \cdot \bar{\boldsymbol{\theta}}] \\ &-(\boldsymbol{\lambda}, \mathbf{w} - \bar{\mathbf{w}} - \bar{\boldsymbol{\theta}} \times (\mathbf{x}^s - \bar{\mathbf{x}})) = 0, \end{aligned} \tag{3.30}$$

and

$$(\boldsymbol{\mu}, \mathbf{v} - \bar{\mathbf{v}} - \bar{\boldsymbol{\omega}} \times (\mathbf{x}^s - \bar{\mathbf{x}})) = 0, \forall \boldsymbol{\mu} \in [H^1(\Omega_s)]^d, \tag{3.31}$$

where the inner product is defined as

$$(\boldsymbol{\mu}, \boldsymbol{\lambda}) = \int_{\Omega_s} (\mu_i \lambda_i + l^2 \mu_{i,j} \lambda_{i,j}) d\Omega, \tag{3.32}$$

with a scaling factor l dependent of the characteristic length of Ω_s.

Remark 3.5 *For clarity, we provide the general variational equations. Just as the treatment for the pressure and the continuity equation, which will be discussed in the following sections, the addition of the distributed Lagrangian multiplier $\boldsymbol{\lambda}$ forms a mixed formulation in which the mixed finite elements must also satisfy the inf-sup conditions [48] [49].*

Remark 3.6 *By comparing the fictitious domain method with the immersed boundary method, the extended immersed boundary method, the immersed finite element method, or the immersed continuum method, it is not difficult to identify the force density $\mathbf{f}^s + m\ddot{\mathbf{u}}_s$ for the immersed boundary or $\mathbf{f}^s$ for the immersed body (continuum), in fact it represents the Lagrangian multiplier for the constraint of Eq. (3.29).*

A clear advantage of the fictitious domain method is the use of the implicit formulation which does not involve the derivative of the delta function. Never-

theless, such a formulation is limited to immersed rigid bodies. In addition, for incompressible viscous fluids, velocity/pressure formulation must also be used along with the distributed Lagrangian multiplier. A wealth of theoretical studies on the inf-sup conditions are available in the context of the treatment of incompressible solids and fluids. In particular, the inf-sup conditions for such a three-field mixed formulation similar to the discussion in Ref. [48] must be considered.

4 Immersed Continuum Method Formulation

In this paper, we present the velocity/pressure formulation for the compressible viscous fluid and the displacement/pressure formulation for the compressible solid with a hyperelastic material model. For simplicity, in this section, we omit the superscript or subscript f for fluid variables.

For the fluid domain, we adopt an Eulerian kinematic description, therefore, the material derivative of the fluid velocity is expressed as

$$\dot{v}_i = v_{i,t} + v_j v_{i,j}. \tag{4.33}$$

Although we refer to the fixed background fluid mesh, we can also employ the arbitrary Lagrangian-Eulerian (ALE) kinematic description [50] [22] and replace the convective velocity in Eq. (4.33) with $\mathbf{v} - \mathbf{v}^m$, where $\mathbf{v}^m$ stands for the given mesh velocity.

For the solid domain, we employ a Lagrangian kinematic description, thus the fluid-solid interface will be tracked automatically by the position of solid particles. Moreover, there is no need for convective terms in the solid domain and the material derivative is the same as the time derivative. Hence, the solid velocity vector $\mathbf{v}^s$ and the acceleration vector $\dot{\mathbf{v}}^s$ can be expressed as

$$\mathbf{v}^s = \dot{\mathbf{u}}^s \text{ and } \dot{\mathbf{v}}^s = \ddot{\mathbf{u}}^s, \tag{4.34}$$

with the displacement vector $\mathbf{u}^s(t) = \mathbf{x}^s(t) - \mathbf{x}^s(0)$, where $\mathbf{x}^s(t)$ and $\mathbf{x}^s(0)$ stand for the current and the original material point positions within the solid domain Ω_s.

We must also point out that the solid domain Ω_s and the material point position $\mathbf{x}^s$ all refer to the current solid configurations, and therefore for clarity could be denoted as $\Omega_s(t)$ and $\mathbf{x}^s(t)$, respectively.

In order to deal with the compressible viscous fluid, we subtract the pressure p from the stress components σ_{ij} to obtain the deviatoric stress components τ_{ij}, which is illustrated in a Newtonian fluid model,

$$\sigma_{ij} = -p\delta_{ij} + \tau_{ij}, \tag{4.35}$$

with $\tau_{ij} = \mu(v_{j,i} + v_{i,j})$.

Furthermore, to couple with the unknown pressure, the continuity equation of the compressible viscous fluid is expressed as

$$v_{i,i} + \frac{\dot{p}}{\kappa} = 0, \tag{4.36}$$

where κ is the bulk modulus of the fluid; and the material derivative $\dot{p}$ can be simply expressed as $p_{,t} + v_i p_{,i}$.

Notice that the compressibility κ in the fluid can be simply viewed as a penalty term associated with the divergence of the fluid velocity. Therefore, for convenience, we ignore the convective term of the pressure and obtain $p_{,t} = \dot{p}$. Furthermore, for typical fluids, we ignore the change of the fluid density due to the pressure change.

Like the fluid stress tensor, we also decompose the solid stress tensor as a hydrostatic pressure p^s, and a deviatoric stress tensor τ^s_{ij},

$$\sigma^s_{ij} = -p^s\delta_{ij} + \tau^s_{ij}. \tag{4.37}$$

Unlike the fluid domain, since we use the Lagrangian description for the submerged solid, the treatments of the continuity equation and the Cauchy stress in nonlinear solid mechanics are not as straightforward. As a special case, if the submerged solid is a flexible structure with a linear elastic material law, we will only have the geometrical nonlinearity to deal with. In this case, suppose the Young's modulus and the Poisson ratio are E and ν, respectively, and the bulk modulus for the solid can be simply expressed as $\kappa^s = E/3(1-2\nu)$.

In this work, we discuss a nonlinear solid mechanics model with both the geometrical and material nonlinearities [45] [46]. First of all, we must introduce the solid deformation gradient $F_{ij} = \partial x^s_i(t)/\partial x^s_j(0)$, from which we can derive the Green-Lagrangian strain ϵ_{ij}. To obtain the energy conjugate stress S_{ij}, the second Piola-Kirchhoff stress, we must first introduce the elastic energy $\bar{W}$, which is often related to the three invariants of the Cauchy-Green deformation tensor $\mathbf{C}$ defined as $\mathbf{F}^T\mathbf{F}$. Moreover, an elastic energy term $-[p^s + \kappa^s(J_3 -$

$1)]^2/2\kappa^s$ is added to $\bar{W}$, along with the solid unknown pressure p^s introduced as

$$J_3 - 1 + \frac{p^s}{\kappa^s} = 0, \tag{4.38}$$

where κ^s is the solid bulk modulus and J_3 stands for the determinant of the deformation gradient.

Of course, to match with the expression in Eq. (4.37), the solid Cauchy stress is converted from the second Piola-Kirchhoff stress,

$$\sigma^s_{ij} = \frac{1}{\det(\mathbf{F})} F_{i,m} S_{mn} F_{j,n}. \tag{4.39}$$

Finally, since the solid displacement is dependent on the fluid velocity, the primary unknowns for the coupled fluid-solid system are the fluid velocity $\mathbf{v}$, the fluid pressure p, and the solid pressure p^s.

Define the Sobolev spaces, so the weak form of governing equations can be modified as: $\forall q \in L^2(\Omega)$, $q^s \in L^2(\Omega_s)$, $\mathbf{w} \in [H^1_{0,\Gamma_v}(\Omega)]^d$, which includes $\forall \mathbf{w}^s \in [H^1(\Omega_s)]^d$, and find $\mathbf{v}$ and $p \in \Omega$, $p^s \in \Omega_s$, such that

$$\begin{aligned}
&\int_\Omega w_i \rho(\dot{v}_i - g_i) d\Omega + \int_\Omega (w_{i,j}\tau_{ij} - p w_{i,i}) d\Omega - \int_{\Gamma_f} w_i f_i^{\Gamma_f} d\Gamma \\
&+ \int_{\Omega_s} [w^s_i(\rho_s - \rho)(\dot{v}_i - g_i) + w^s_{i,j}(\tau^s_{ij} - \tau^f_{ij}) - (p^s - p) w^s_{i,i}] d\Omega + \\
&+ \int_\Omega q(v_{j,j} + \frac{p_{,t}}{\kappa}) d\Omega + \int_{\Omega_s} q^s (J_3 - 1 + \frac{p^s}{\kappa^s}) d\Omega = 0.
\end{aligned} \tag{4.40}$$

Note that within the domain Ω_s the fluid stress τ^f_{ij} is calculated with the fluid formulation. Using integration by parts and the divergence theorem, we establish the following strong form:

$$\rho_s \dot{v}^s_i = -p^s_{,i} + \tau^s_{ij,j} + \rho_s g_i, \text{ in } \Omega_s, \tag{4.41}$$
$$p^s = -\kappa^s (J_3 - 1), \tag{4.42}$$
$$\rho \dot{v}_i = -p_{,i} + \tau_{ij,j} + \rho g_i, \text{ in } \Omega_f, \tag{4.43}$$
$$p_{,t} = -\kappa v_{j,j}, \tag{4.44}$$
$$[v_i] = 0, \text{ on } \Gamma_s, \text{ kinematic matching}, \tag{4.45}$$
$$[\sigma_{ij} n_j] = 0, \text{ on } \Gamma_s, \text{ dynamic matching}, \tag{4.46}$$

where the surface normal vector $\mathbf{n}$ is aligned with that of the solid domain $\mathbf{n}^s$

and is opposite to that of the fluid domain $\mathbf{n}^f$.

We recognize that there are two sets of discretizations, namely, one for the Lagrangian solid mesh and the other one for the Eulerian fluid mesh. In this paper, the discretization of the fluid domain is identical to the stabilized Galerkin formulation for the Navier-Stokes equations [51] [43] [44]. It is clear that different numerical schemes for fluid flows such as the flow-condition-based interpolation finite element scheme [52] or the lattice Boltzmann method [53] can also be employed in the immersed continuum method as the fluid solver.

In this paper, we introduce for the fluid domain the following interpolations for the entire domain Ω:

$$\mathbf{v}^h = N_I^v \mathbf{v}_I,\ \mathbf{w}^h = N_I^v \mathbf{w}_I,\ p^h = N_I^p p_I,\ q^h = N_I^p q_I, \tag{4.47}$$

where N_I^v and N_I^p stand for the interpolation functions at node I for the velocity vector and the pressure; and $\mathbf{v}_I$, $\mathbf{w}_I$, p_I, and q_I are the nodal values of the discretized velocity vector, admissible velocity variation, pressure, and pressure variation, respectively.

Notice that in general the interpolation functions for the velocity vector and the unknown pressures are different. Therefore, we retain the superscripts v and p to denote such differences. Furthermore, we ignore the change of the fluid density due to the pressure change.

Likewise for the solid domain Ω_s, the discretization is based on the following:

$$\mathbf{u}^{s,h} = N_J^u \mathbf{u}_J^s,\ \mathbf{w}^{s,h} = N_J^u \mathbf{w}_J^s,\ p^{s,h} = N_J^{p^s} p_J^s,\ q^{s,h} = N_J^{p^s} q_J^s, \tag{4.48}$$

where N_J^u and $N_J^{p^s}$ stand for the interpolation functions at node J for the displacement vector and the unknown pressures; and $\mathbf{u}_J^{s,h}$, $\mathbf{w}_J^{s,h}$, $p_J^{s,h}$, and $q_J^{s,h}$ are the nodal values of the discretized displacement vector, admissible velocity variation, pressure, and pressure variation, respectively.

Substituting both discretizations (4.47) and (4.48) into Eq. (4.40), we obtain the following discretization of the weak form: $\forall q^h \in L^2(\Omega^h)$, $q^{s,h} \in L^2(\Omega_s^h)$, $\mathbf{w}^h \in [H^{1,h}_{0,\Gamma_v^h}(\Omega^h)]^d$, which includes $\forall \mathbf{w}^{s,h} \in [H^{1,h}(\Omega_s^h)]^d$,

$$\int_{\Omega^h} w_{iI} N_I^v \rho \dot{v}_i^h d\Omega - \int_{\Gamma_f^h} w_{iI} N_I^v f_i^{\Gamma_f^h} d\Gamma + \int_{\Omega^h} (w_{iI} N_{I,j}^v \tau_{ij} - p^h w_{iI} N_{I,i}^v) d\Omega$$
$$+ \int_{\Omega_s^h} [w_{iJ}^s N_J^u (\rho_s - \rho)(\dot{v}_i^h - g_i) + w_{iJ}^s N_{J,i}^u (\sigma_{ij}^s - \sigma_{ij}^f)] d\Omega - \int_{\Omega^h} w_{iI} N_I^v \rho g_i d\Omega$$
$$+ \int_{\Omega^h} q_I N_I^p (v_{j,j}^h + \frac{p_{,t}^h}{\kappa}) d\Omega + \int_{\Omega_s^h} q_J^s N_J^{p^s} (J_3 - 1 + \frac{p^{s,h}}{\kappa^s}) d\Omega = 0. \tag{4.49}$$

The key of the immersed continuum method is to recognize the fact that the nonlinear mapping from $\mathbf{w}_I$ to $\mathbf{w}_J^s$, namely, from the fluid mesh to the solid mesh is derived from the discretized constraint of the velocities of the immersed solid and the corresponding fluid occupying the same solid domain. It turns out that such discretized mapping using various kernel functions has been studied recently in the meshless finite element methods. For example, the reproducing kernel particle method (RKPM) was proposed as an alternative or enhancement to various numerical procedures including finite element methods (Liu *et al.*, 1995 and 1996, [54] [55] [56] and Li and Liu, 1999 [57]). Unlike the discretized delta function in the immersed boundary method [58], the kernel functions in the meshless methods can handle non-uniform meshing, which marks an important improvement for the increase of the local resolutions near the interfaces. Furthermore, the adjustable reproducing properties of the meshless kernels enable a better representation of the discretized delta function in the frequency domain, namely, as the polynomial order $n \to \infty$, the discretized delta function ϕ becomes flatter at $\omega = 0$ and approaches to an ideal filter in the frequency domain. A detailed discussion of the delta function can be found in Refs. [45] [46].

Hence, at a typical solid node J, with a finite support domain Ω_J, the discretized form of the constraint of the velocities of the immersed solid and the corresponding fluid occupying the same solid domain can be expressed as

$$\mathbf{v}_J^s = \sum_I \mathbf{v}_I \phi_I(\mathbf{x}_I - \mathbf{x}_J^s) \text{ and } \mathbf{w}_J^s = \sum_I \mathbf{w}_I \phi_I(\mathbf{x}_I - \mathbf{x}_J^s), \forall \mathbf{x}_I \in \Omega_J, \tag{4.50}$$

where $\phi_I(\mathbf{x}_I - \mathbf{x}_J)$ is the kernel function centered at the solid node J, represented with $\mathbf{x}_J^s$.

It is very important to realize that the material points of the submerged solid domain will move in the entire domain, therefore even if we do not adjust the size of the support domain attached to these material points, Eq. (4.50) represents a nonlinear mapping which in this work for convenience is simply

denoted as $\tilde{N}$.

Note that in general within the solid domain, we can ignore the stress components computed using the fluid model. If however we want to include the stress difference $\sigma_{ij}^s - \sigma_{ij}^f$ within the solid mesh, in addition to the mapping of the velocity vector in Eq. (4.50). In order to use the definition of σ_{ij}^f, we must also map the unknown pressure from the fluid mesh denoted with node I to the solid mesh denoted with node J. Therefore, like Eq. (4.50), we have

$$p_J^f = \sum_I p_I \phi_I(\mathbf{x}_I - \mathbf{x}_J), \forall \mathbf{x}_I \in \Omega_J. \tag{4.51}$$

Remark 4.1 *In the immersed continuum method, we employ implicit time integration, therefore there is no need to explicitly express the so-called equivalent fluid-structure interaction forces. In fact, the beauty of the immersed continuum method is simply a nonlinear mapping of the velocity and the unknown pressures between the two media within the submerged domain Ω_s through various meshless kernel functions.*

Therefore, for the entire domain Ω, due to the arbitrariness of the variations w_{iI}, q_I, and q_J^s, we have four equations at each fluid node I and one equation at each solid node J,

$$r_{iI}^v = 0,\ r_I^p = 0,\ r_J^{p^s} = 0, \tag{4.52}$$

where the residuals are defined as

$$\begin{aligned}
r_{iI}^v &= \int_{\Omega^h} N_I^v \rho \dot{v}_i^h d\Omega + \int_{\Omega^h} [N_{I,j}^v \tau_{ij} - p^h N_{I,i}^v] d\Omega - \int_{\Gamma_f^h} N_I^{v,\Gamma_f^h} f_i^{\Gamma_f^h} d\Gamma \\
&\quad + \int_{\Omega_s^h} \tilde{N}[N_J^u(\rho_s - \rho)(\dot{v}_i^h - g_i) + N_{J,i}^u(\sigma_{ij}^s - \sigma_{ij}^f)] d\Omega - \int_{\Omega^h} N_I^v \rho g_i d\Omega, \\
r_I^p &= \int_{\Omega^h} N_I^p (v_{j,j}^h + \frac{p_{,t}^h}{\kappa}) d\Omega, \\
r_J^{p^s} &= \int_{\Omega_s^h} N_J^{p^s} (J_3 - 1 + \frac{p^{s,h}}{\kappa^s}) d\Omega.
\end{aligned} \tag{4.53}$$

Note that the convective terms are hidden in $\dot{v}_i^h$ and the detailed expressions of the stabilized Galerkin formulation for the Navier-Stokes equations are identical to those employed in the immersed finite element method [46].

For clarity, we introduce a displacement vector $\mathbf{u}$, although it is only evaluated

in the solid domain Ω_s in which a Lagrangian description is prescribed. In fact, within the solid domain, $\mathbf{u}$ is denoted as $\mathbf{u}^s$ and evolves based on $\mathbf{v}^s$ and $\dot{\mathbf{v}}^s$ which are the fluid velocity and acceleration vectors $\mathbf{v}$ and $\dot{\mathbf{v}}$ directly evaluated at the material point $\mathbf{x}^s$. Moreover, in the discussion of numerical procedures, we denote the time derivative of a variable a as $\dot{a}$. Denote the residuals in Eq. (4.53) as $\mathbf{r}^T = (\mathbf{r}^{v\,T}, \mathbf{r}^{p\,T}, \mathbf{r}^{p^s\,T})$, we obtain the following nonlinear equation

$$\mathbf{r}(\mathbf{u}, \mathbf{v}, \dot{\mathbf{v}}, p, \dot{p}, p^s) = \mathbf{0}. \tag{4.54}$$

The details of the fully implicit time integration with a matrix-free combination of Newton-Raphson and GMRES iterative procedures in the solution of Eq. (4.54) are presented in Ref. [59].

5 Numerical Examples

In this section, we present a set of numerical examples. In the first example, a deformable cylinder or disk with a diameter of $2a$ is released to fall in a viscous fluid channel with a dimension of $2L \times 8L$. The physical parameters of this case are given as follows: gravitational constant $g = 9.81\ m/s^2$; dynamic viscosity $\mu = 1\ dyne/cm^2 \cdot s$; fluid density $\rho_f = 1\ g/cm^3$; and $L = 2\ cm$. To implement the effect of gravity, an external body force is only applied to the cylinder. The buoyancy is captured by the definition of the mass matrix. If the cylinder is rigid, the terminal velocity can be expressed as, according to Ref. [60],

$$U = \frac{(\rho_s - \rho_f) g a^2}{4\mu} \left[\ln(\frac{L}{a}) - 0.9157 + 1.7244(\frac{a}{L})^2 - 1.7302(\frac{a}{L})^4 \right]. \tag{5.55}$$

With a diameter ratio $a/L = 0.25$, the theoretical terminal velocity of the rigid cylinder compares well with the computational result. Moreover, by replacing the discretized delta function of the immersed boundary method with a cubic spline, we seem to obtain more accurate solutions. This improvement is more visable for coarse grids.

In Fig. 2, it is clearly shown that the deformation of the submerged solid has a significant effect on the terminal velocity. In general, the flexibility of the cylinder decreases the surrounding fluid forces (viscous shear, form drag, etc.) and as a consequence increases the terminal velocity. In this example, the submerged solid is made of an almost incompressible rubber material with the

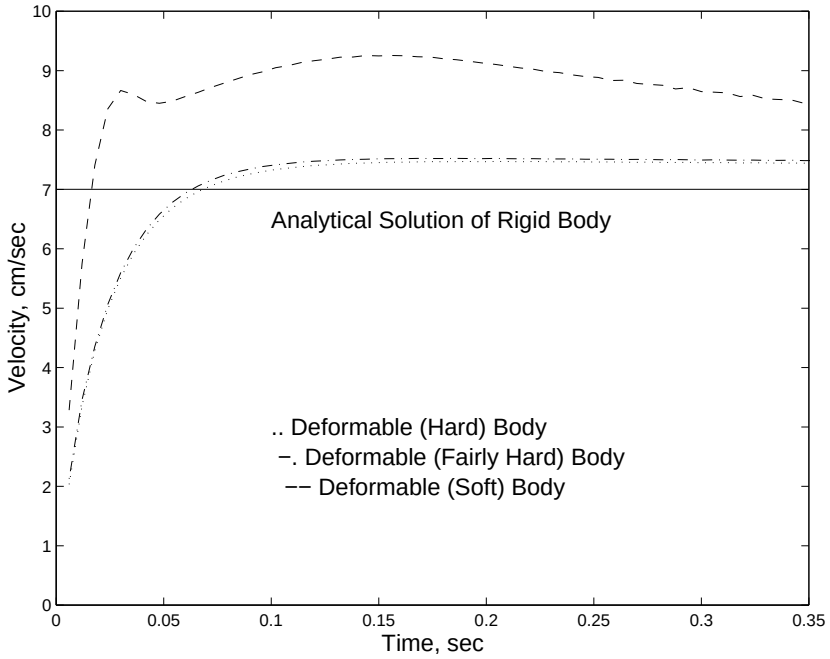

Fig. 2. The velocity history of a moving object with a diameter ratio $a/L = 0.25$ and a 64×256 fluid grid.

material constants $C_1 = 29300$, $C_2 = 17700$, and $\kappa = 141000\ dyne/cm^2$ and the density $\rho_s = 3\ g/cm^3$.

In the second example, one viscous fluid is injected into another viscous fluid. Due to the surface tension effects, viscous fluid exiting the tube tends to form a droplet. Some preliminary simulation results are illustrated in Fig. 3.

The third example demonstrating the capability of the proposed method is the transport of multiple normal and sickle red blood cells through micro-vessels. This complex three-dimensional model as illustrated in Fig.4 is virtually impossible to tackle with existing modelling techniques. The detailed study along with the embedded multi-scale modeling of cell-cell interactions have already been published in Ref. [61].

In another numerical test, a chain of three deformable objects are released and move towards to an elastic bifurcation. Initially, these objects are perfectly centered and aligned with the bifurcation point. What breaks the symmetry is the slight difference between the upper and lower branches of the bifurcation. As shown in Fig. 6, objects impact, deform, and conform with the viscous flow within the lower branch of the bifurcation. This type of study is very important for the understanding of the adverse effects of artificial devices exerted on red blood cells.

Finally, in the simple setup as illustrated in the preliminary comparison in Fig. 5, the simulation results are very much the same as the experimental

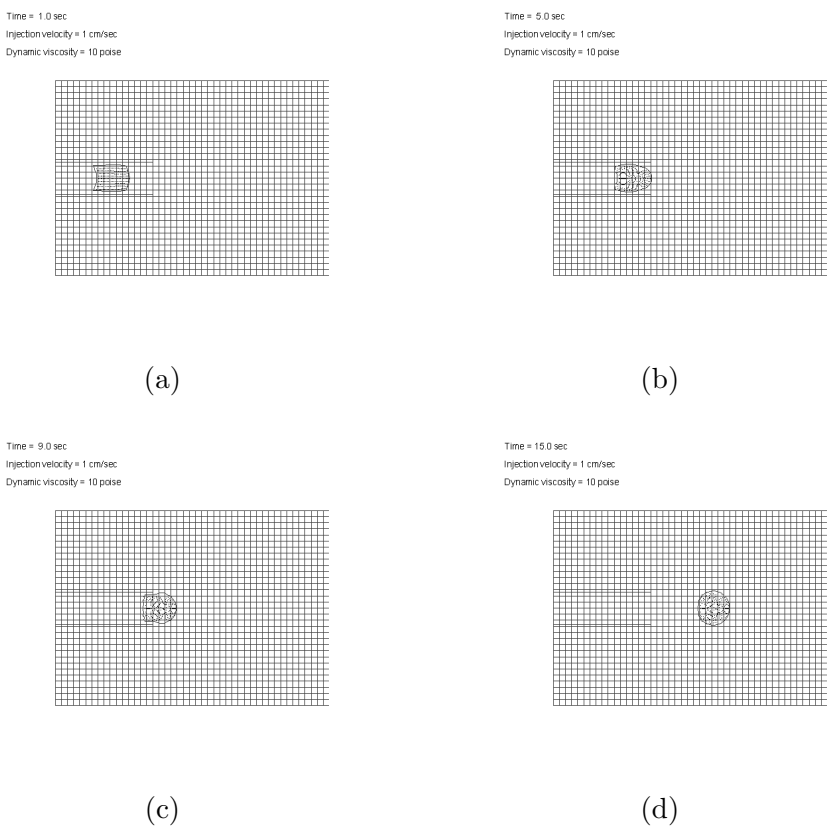

Fig. 3. One viscous fluid injected into another viscous fluid.

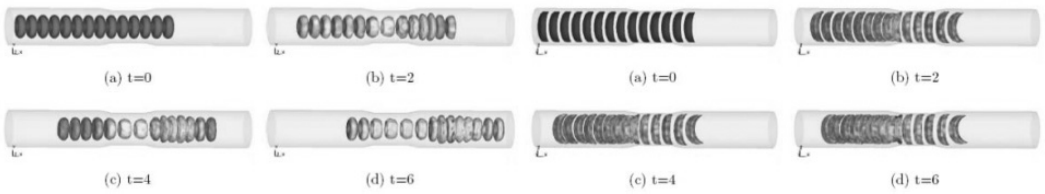

Fig. 4. Normal and sickle red blood cells passing through a micro-vessel constriction.

observation at individual time steps. In the experiment, water was pulsed through a column with a square cross section ($5x5$ cm) at a frequency of 1 Hz. A rubber shell-like structure was located inside this column. In the simulation both velocity vectors of the fluid flow and stress tensors of the flexible structure are captured for the entire fluid and solid domains, whereas the preliminary experimental observation can only provide us with the dynamic behavior of the structure as well as overall flow patterns. This in fact brings up an important point that is for the actual valve design simulation tools are very much required since many areas of the valve are difficult to visualize and only limited amounts of data can be collected experimentally.

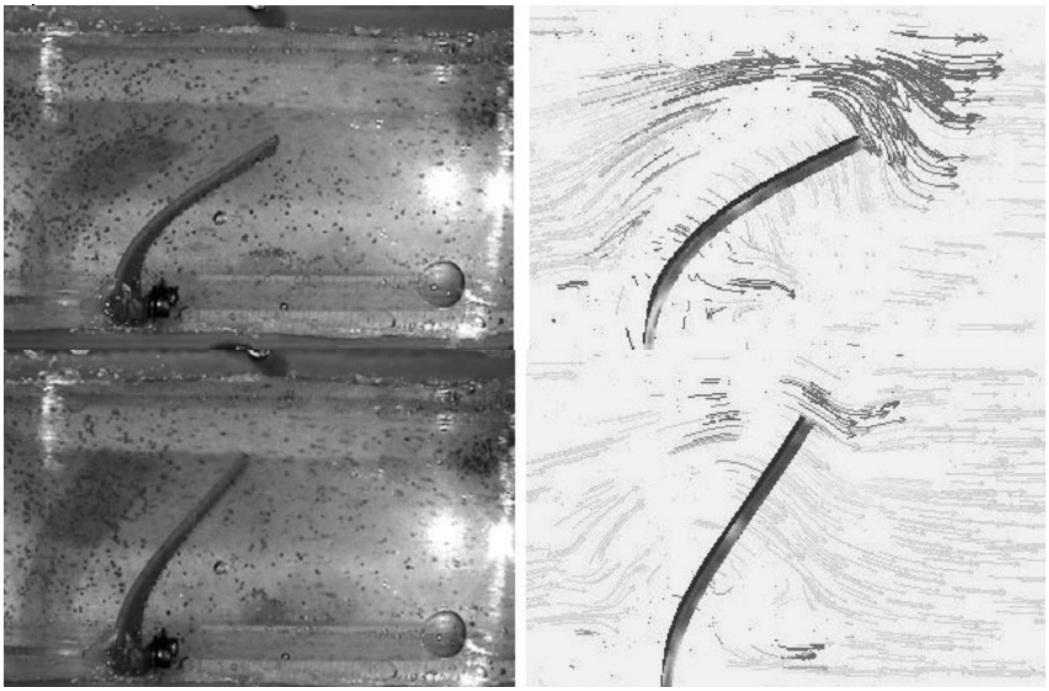

Fig. 5. A preliminary comparison between experimental observation and computer simulation of a three-dimensional shell-like structure deflecting in a pulsatile flow through a square cross-sectional channel.

6 Conclusion

The coupling of fluids and solids is the central feature in the study of the mechanics of the heart, arteries, veins, microcirculation, and pulmonary blood flow. Currently, the modelling of strong hemodynamic interaction with flexible structures is limited by severe fluid mesh distortions around flexible structures with large deformations and displacements. Recent breakthrough has been made in the development of extended immersed boundary method (EIBM) [45], immersed finite element method (IFEM) [46], and immersed continuum method (ICM) [59]. In particular both EIBM and IFEM are based on the explicit time integration for the fluid-solid coupling and deal exclusively with immersed incompressible materials interacting with surrounding incompressible fluid. The difference between EIBM and IFEM is that in EIBM, a spectral fluid solver is used with a uniform background grid, whereas in IFEM, a finite element fluid solver is adopted with a non-uniform finite element mesh. Unlike the immersed boundary method, which handles only volumeless immersed fibers, the newly developed methods (EIBM, IFEM, and ICM) deal with immersed continua occupying finite volumes within the surrounding fluid medium. Furthermore, in ICM, compressible solid will be able to couple with compressible fluid in a fully implicit formulation. In essence, the new modelling methods adopt an independent solid mesh moving on top of a fixed or prescribed arbitrary Lagrangian-Eulerian (ALE) background fluid mesh. This is a

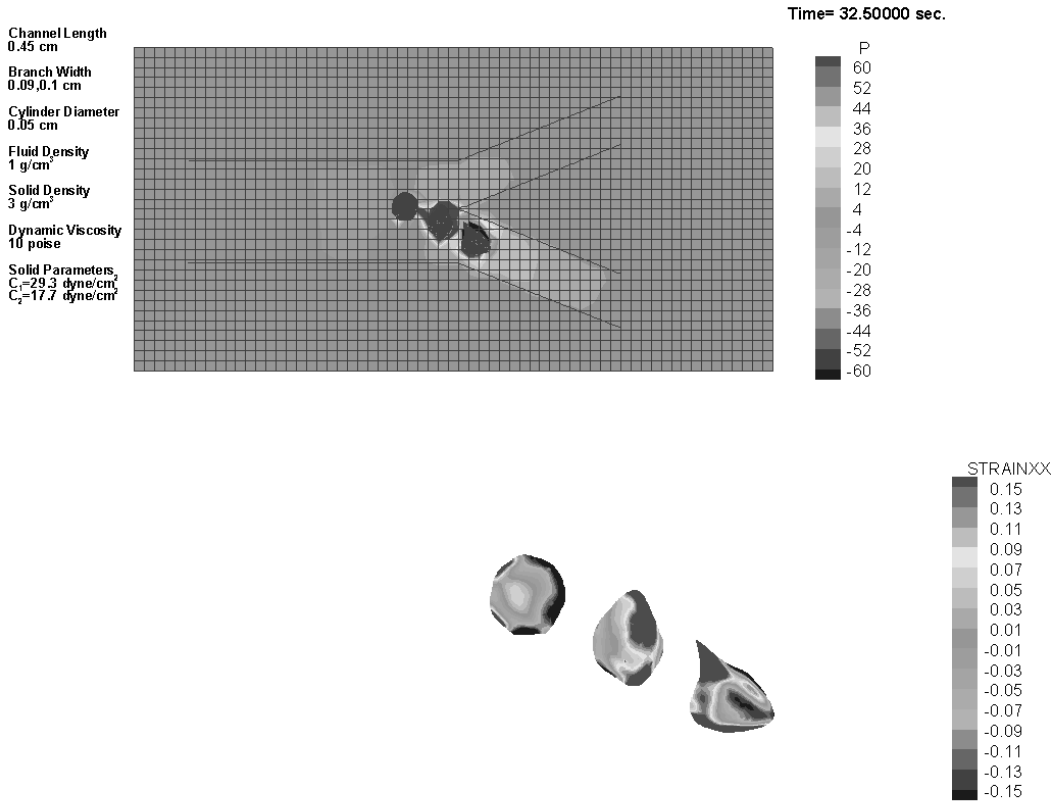

Fig. 6. Three deformable objects impact the elastic bifurcation point and conform to the flow within the lower branch.

new and effective strategy in dealing with fluid-structure interaction problems. Rather than identify and follow the fluid-structure interfaces, we substitute the entire submerged solids with a collection of immersed Lagrangian nodal points, and as a consequence, automatically define the interfaces with the material points enclosing the solid domains. This method promises to provide an easy treatment of complex fluid-solid systems and hence a platform or linkage for multi-scale and multi-physics modelling of biological systems.

7 Acknowledgment

The author would like to thank Professor W.K. Liu and his research group at Northwestern University for their help during the preparation of this manuscript. The supports from NASA Langley and NSF (DMI-0503652 and BES-0503649) are greatly acknowledged.

References

[1] O.C. Zienkiewicz and R.E. Newton. Coupled vibrations of a structure submerged in a compressible fluid. *Proc. Symp. Finite Element Techniques*, pages 359–379, 1969. University of Stuttgart, Germany.

[2] C.C. Mei. Numerical methods in water-wave diffraction and radiation. *Annual Review of Fluid Mechanics*, 10:393–416, 1978.

[3] J.A. Aranha, C.C. Mei, and D.K.P. Yue. Some properties of a hybrid element method for water waves. *International Journal for Numerical Methods in Engineering*, 14:1627–1641, 1979.

[4] L. Kiefling and G.C. Feng. Fluid-structure finite element vibrational analysis. *AIAA Journal*, 14:199–203, 1976.

[5] M.A. Hamdi, Y. Ousset, and G. Verchery. A displacement method for the analysis of vibrations of coupled fluid-structure systems. *International Journal for Numerical Methods in Engineering*, 13:139–150, 1978.

[6] L.G. Olson and K.J. Bathe. A study of displacement-based fluid finite elements for calculating frequencies of fluid and fluid-structure systems. *Nuclear Engineering and Design*, 76:137–151, 1983.

[7] H.C. Chen and R.L. Taylor. Vibration analysis of fluid-solid systems using a finite element displacement formulation. *International Journal for Numerical Methods in Engineering*, 29:683–698, 1990.

[8] H.J.P. Morand and R. Ohayon. Substructure variational analysis of the vibrations of coupled fluid-structure systems. Finite element results. *International Journal for Numerical Methods in Engineering*, 14:741–755, 1979.

[9] G.C. Everstine. A symmetric potential formulation for fluid-structure interaction. *Journal of Sound and Vibration*, 79:157–160, 1981.

[10] L.G. Olson and K.J. Bathe. Analysis of fluid-structure interactions. A direct symmetric coupled formulation based on the fluid velocity potential. *Computers & Structures*, 21(1/2):21–32, 1985.

[11] C.A. Felippa and R. Ohayon. Mixed variational formulation of finite element analysis of acoustoelastic/slosh fluid-structure interaction. *Journal of Fluids and Structures*, 4:35–57, 1990.

[12] X. Wang and K.J. Bathe. Displacement/pressure based finite element formulations for acoustic fluid-structure interaction problems. *International Journal for Numerical Methods in Engineering*, 40:2001–2017, 1997.

[13] T.B. Belytschko and J.M. Kennedy. A fluid-structure finite element method for the analysis of reactor safety problems. *Nuclear Engineering and Design*, 38:71–81, 1976.

[14] T.B. Belytschko. Fluid-structure interaction. *Computers & Structures*, 12:459–469, 1980.

[15] K.C. Park. Partitioned transient analysis procedures for coupled-field problems: Stability analysis. *Journal of Applied Mechanics*, 47:370–376, 1980.

[16] T.B. Belytschko and R. Mullen. Two-dimensional fluid-structure impact computations with regularization. *Computer Methods in Applied Mechanics and Engineering*, 27:139–154, 1981.

[17] W.K. Liu. Finite element procedures for fluid-structure interactions and application to liquid storage tanks. *Nuclear Engineering and Design*, 65:221–238, 1981.

[18] T.E. Tezduyar, M. Behr, and J. Liou. A new strategy for finite element computations involving moving boundaries and interfaces-The DSD/ST procedure: I. The concept and the preliminary numerical tests. *Computer Methods in Applied Mechanics and Engineering*, 94:339–351, 1992.

[19] T. Nomura and T.J.R. Hughes. An arbitrary Lagrangian-Eulerian finite element method for interaction of fluid and a rigid body. *Computer Methods in Applied Mechanics and Engineering*, 95:115–138, 1992.

[20] C. Farhat, M. Lesoinne, and N. Maman. Mixed explicit/implicit time integration of coupled aeroelastic problems: Three-field formulation, geometric conservation and distributed solution. *International Journal for Numerical Methods in Fluids*, 21:807–835, 1995.

[21] K.J. Bathe. Simulation of structural and fluid flow response in engineering practice. *Computer Modeling and Simulation in Engineering*, 1:47–77, 1996.

[22] X. Wang. Velocity/Pressure mixed finite element and finite volume formulation with ALE descriptions for nonlinear fluid-structure interaction problems. *Advances in Engineering Software*, 31:35–44, 2000.

[23] H. Morand and R. Ohayon. *Fluid Structure Interaction - Applied Numerical Methods*. John Wiley & Sons, 1995. Translated by C.A. James.

[24] K.J. Bathe. Simulation of structural and fluid flow response in engineering practice. *Computer Modeling and Simulation in Engineering*, 1:47–77, 1996.

[25] K.J. Bathe. Fluid-structure interactions - The fully coupled solution of fluid flows with structural interactions, a rapidly evolving discipline, represents the natural next step in simulating mechanical systems. *Journal of Mechanical Engineering*, pages 66–68, April 1998.

[26] S. Piperno, C. Farhat, and B. Larrouturou. Partitioned procedures for the transient solution of coupled aeroelastic problems - Part I: Model problem, theory and two-dimensional application. *Computer Methods in Applied Mechanics and Engineering*, 124:79–112, 1995.

[27] O. Ghattas and X. Li. A variational finite element method for stationary nonliear fluid-solid interaction. *Journal of Computational Physics*, 121:347–356, 1995.

[28] O. Ghattas and X. Li. Domain decomposition methods for sensitivity analysis of a nonlinear aeroelasticity problem. *Journal of Computational Physics*, 11:113–130, 1998.

[29] C.S. Peskin. Numerical analysis of blood flow in the heart. *Journal of Computational Physics*, 25:220–252, 1977.

[30] D.M. McQueen and C.S. Peskin. Computer-assisted design of butterfly bileaflet valves for the mitral position. *Scand. J. Thor. Cardiovasc. Surg.*, 19:139–148, 1985.

[31] L.J. Fauci and C.S. Peskin. A computational model of aquatic animal locomotion. *Journal of Computational Physics*, 77:85–108, 1988.

[32] J.M. Stockie and B.R. Wetton. Analysis of stiffness in the immersed boundary method and implications for time-stepping schemes. *Journal of Computational Physics*, 154:41–64, 1999.

[33] Jr. R.P. Beyer. A computational model of the cochlea using the immersed boundary method. *Journal of Computational Physics*, 98:145–162, 1992.

[34] R. Dillon, L. Fauci, A. Fogelson, and D. Gaver III. Modeling biofilm processes using the immersed boundary method. *Journal of Computational Physics*, 129:57–73, 1996.

[35] R.J. LeVeque and Z.L. Li. Immersed interface methods for Stokes flow with elastic boundaries or surface tension. *SIAM Journal on Scientific Computing*, 18:709–735, 1997.

[36] J.A. Sethian. *Level Set Methods and Fast Marching Methods.* Cambridge University Press, 1996.

[37] A.-K. Tornberg and M. Shelley. Simulating the dynamics and interactions of flexible fibers in stokes flows. *Journal of Computational Physics*, 196:8–40, 2004.

[38] S. Alben, M. Shelley, and J. Zhang. Drag reduction through self-similar bending of a flexible body. *Nature*, 420:479–481, 2002.

[39] C. Yang, D. Tang, and S.Q. Liu. A multi-physics growth model with fluid-structure interactions for blood flow and re-stenosis in rat vein grafts. *Computers & Structures*, 81:1041–1058, 2003.

[40] Z.J. Wang, J. Birch, and M. Dickinson. Unsteady forces and vorticity field in hovering flight: Two dimensional computations vs robotic wing experiments. *J. Exp. Biol.*, 207:449–460, 2004.

[41] T.J.R. Hughes, W.K. Liu, and T.K. Zimmerman. Lagrangian-Eulerian finite element formulations for incompressible viscous flows. *Computer Methods in Applied Mechanics and Engineering*, 29:329–349, 1981.

[42] K.J. Bathe, H. Zhang, and M.H. Wang. Finite element analysis of incompressible and compressible fluid flows with free surfaces and structural interactions. *Computers & Structures*, 56(2/3):193–213, 1995.

[43] T.E. Tezduyar. Stabilized finite element formulations for incompressible-flow computations. *Advances in Applied Mechanics*, 28:1–44, 1992.

[44] T.E. Tezduyar. Finite element methods for flow problems with moving boundaries and interfaces. *Archives of Computational Methods in Engineering*, 8:83–130, 2001.

[45] X. Wang and W.K. Liu. Extended immersed boundary method using FEM and RKPM. *Computer Methods in Applied Mechanics and Engineering*, 193:1305–1321, 2004.

[46] L. Zhang, A. Gerstenberger, X. Wang, and W.K. Liu. Immersed finite element method. *Computer Methods in Applied Mechanics and Engineering*, 193:2051–2067, 2004.

[47] R. Glowinski, T.W. Pan, T.I. Hesla, D.D. Joseph, and J. Périaux. A fictitious domain approach to the direct numerical simulation of incompressible viscous flow past moving rigid bodies: Application to particulate flow. *Journal of Computational Physics*, 169:363–426, 2001.

[48] W. Bao, X. Wang, and K.J. Bathe. On the Inf-Sup condition of mixed finite element formulations for acoustic fluids. *Mathematical Models & Methods in Applied Sciences*, 11:883–901, 2001.

[49] K.J. Bathe. *Finite Element Procedures*. Prentice Hall, Englewood Cliffs, N.J., 1996.

[50] J. Donea, S. Giuliani, and J.P. Halleux. An arbitrary Lagrangian-Eulerian finite element method for transient dynamic fluid-structure interactions. *Computer Methods in Applied Mechanics and Engineering*, 33:689–723, 1982.

[51] T.J.R. Hughes, L.P. Franca, and M. Balestra. A new finite element formulation for computational fluid dynamics: V. Circumventing the Babuška-Brezzi condition: A stable Petrov-Galerkin formulation of the Stokes problem accommodating equal-order interpolations. *Computer Methods in Applied Mechanics and Engineering*, 59:85–99, 1986.

[52] K.J. Bathe and H. Zhang. Finite element developments for general fluid flows with structural interactions. *International Journal for Numerical Methods in Engineering*, 2004. In press.

[53] Z.G. Feng, X. Wang, and E.E. Michaelides. A new approach to treat the solid-fluid boundary conditions in Lattice Boltzmann method. In *7th US National Congress on Computational Mechanics*, 2003.

[54] W.K. Liu, Y. Chen, C.T. Chang, and T.B. Belytschko. Advances in multiple scale kernel particle methods. *Computational Mechanics*, 18:73–111, 1996.

[55] W.K. Liu, S. Jun, and Y.F. Zhang. Reproducing kernel particle methods. *International Journal for Numerical Methods in Fluids*, 20:1081–1106, 1995.

[56] W.K. Liu and Y.J. Chen. Wavelet and multiple scale reproducing kernel methods. *International Journal for Numerical Methods in Fluids*, 21:901–932, 1995.

[57] S. Li and W.K. Liu. Reproducing kernel hierachical partition of unity part I: Formulation and theory. *International Journal for Numerical Methods in Engineering*, 45:251–288, 1999.

[58] C.S. Peskin. The immersed boundary method. *Acta Numerica*, 11:479–517, 2002.

[59] X. Wang, W.K. Liu, and G. Chen. Immersed continuum method. *International Journal for Numerical Methods in Engineering*, 2004. Submitted.

[60] J. Happel and H. Brenner. *Low Reynolds number hydrodynamics*. Martinus Nijhoff Publishers, 1983.

[61] Y. Liu, L. Zhang, X. Wang, and W.K. Liu. Coupling of Navier-Stokes equations with protein molecular dynamics and its application to hemodynamics. *International Journal for Numerical Methods in Fluids*, 46:1237–1252, 2004.